論文 / 著書情報
Article / Book Information

Title	Multiple-Image-Based Restoration for Motion Blur with Non-uniform Point Spread Function
Authors	Karn Patanukhom, Akinori NISHIHARA
Citation	IEICE Trans. Fundamentals, Vol. E91-A, No. 8, pp. 1924-1934
Pub. date	2008, 8
URL	http://search.ieice.org/
Copyright	(c) 2008 Institute of Electronics, Information and Communication Engineers

IEICE TRANS. FUNDAMENTALS, VOL.E91–A, NO.8 AUGUST 2008

PAPER Special Section on Signal Processing

Multiple-Image-Based Restoration for Motion Blur with Non-uniform Point Spread Function

Karn PATANUKHOM[†a)], *Nonmember and* **Akinori NISHIHARA**[††], *Fellow*

SUMMARY A blind image restoration for non-linear motion blurs with non-uniform point spread functions based on multiple blurred versions of a same scene is proposed. The restoration is separately considered as identification and deconvolution problems. In the proposed identification process, an identification difficulty is introduced to rank an order of blur identification. A blurred image with the lowest identification difficulty is initially identified by using a single-image-based scheme. Then, other images are identified based on a cross convolution relation between each pair of blurred images. In addition, an iterative feedback scheme is applied to improve the identification results. For the deconvolution process, a spatial adaptive scheme using regional optimal terminating points is modified from a conventional iterative deconvolution scheme. The images are decomposed into sub-regions based on smoothness. The regional optimal terminating points are independently assigned to suppress a noise in smooth regions and sharpen the image in edgy regions. The optimal terminating point for each region is decided by considering a discrepancy error. Restoration examples of simulated and real world blurred images are experimented to demonstrate the performance of the proposed method.

key words: *blur identification, motion blur, image restoration, multiple image*

1. Introduction

A motion blur is one of frequently seen types of image degradation caused by relative motions between a camera and objects during exposure time. Restoration for the blurred images has been studied [1]–[12]. An original scene can be restored by using only one blurred image (single-image-based restoration) or by using additional images (multiple-image-based restoration). Most of the single-image-based approaches are limited for identification of simple blur models such as 1D motion models [1]–[3] or constant velocity motion models [1]–[4]. To identify more complex models of blurs, several methods such as auto-regressive (AR) model and maximum likelihood (ML) based methods [5], [6] have been proposed. Although the ML-based approaches can estimate more complex models of blurs by using a single image, there are some practical limitations such as a good prior estimation of a blur length, strong assumptions on image model and noise, and a high computational cost.

Manuscript received December 11, 2007.
Manuscript revised March 1, 2008.

[†]The author is with the Department of Communications and Integrated Systems, Tokyo Institute of Technology, Tokyo, 152-8552 Japan.
[††]The author is with the Center for Research and Development of Educational Technology, Tokyo Institute of Technology, Tokyo, 152-8552 Japan.
a) E-mail: karn@nh.cradle.titech.ac.jp

DOI: 10.1093/ietfec/e91–a.8.1924

On the other hand, multiple-image-based methods can identify more complex motion models without strong assumptions on image models because more information is provided by additional images. In addition, an ill-posed problem appearing in the single-image-based deconvolution approaches tends to become well-posed when more than one blurred image are provided. For identification of complex motion blur models, multiple-image-based approaches have been studied [7]–[10]. Ben-Ezra, et al. [7] proposed an approach that needs an additional sensor to capture an image sequence for estimation of the motion in the scene. Instead of capturing the image sequence, Tico, et al. [8] proposed to capture an additional special shot. To avoid the motion blur in the additional shot, an image with low SNR is captured by using a small exposure time. Then, the blur is identified based on a relation between the two shots. However, the exposure time has to be adjusted for each shot. In addition, the deconvolution processes in [7], [8] are still based on a single image which may suffer from the ill-posed problem. On the other hand, Giannakis, et al. [9] proposed a scheme that reconstructs an original image by using multiple blurred images with a general type of blurs. The multiple blurred image formation and restoration are modeled by a filter bank where a reconstruction filter is equivalent to a synthesis filter bank with a perfect reconstruction property. However, this scheme is not suitable for the cases of motion blur with long motion length because a number of 2-D FIR filter coefficients have to be prepared to model the blur function while most of actual values for the prepared coefficients are zeros according to characteristics of motion blur. Therefore, a number of support coefficients are redundant, which may cause errors. In addition, the complexity also significantly increases due to the number of support coefficients; the scheme is not robust enough for the noises and misalignments in the real situation; and the minimum-norm perfect reconstruction solution may enlarge the noises. More specific scheme which uses two linear motion blurred images with different blur direction was proposed by Rav-Acha, et al. [10]. Since a dimension of the blur function reduces from 2-D to 1-D, more robust and accurate identification scheme can be obtained while the number of unknowns and complexity are less than [9]. However, the scheme is only limited to the linear motion blur model.

In this paper, a more robust and flexible blind image restoration scheme for motion blur using multiple blurred version of the same scene is proposed. The objective of the proposed scheme is to deal with general motion blurs,

including non-linear motion or non-constant velocity motion. The proposed scheme includes both identification and deconvolution algorithms. Details of the proposed identification and deconvolution schemes are presented in Sect. 2 and Sect. 3, respectively. Some experimental examples are demonstrated in Sect. 4. Finally, Sect. 5 gives conclusions of this paper.

2. Identification Scheme Using Blur Identification Difficulty

Based on an assumption that the blur operator is shift-invariant and all blurred images are aligned, the multiple degraded version of the same original scene can be modeled in a spatial domain as

$$g_i(x, y) = h_i * f(x, y) + n_i(x, y), \tag{1}$$

where f and g are original and degraded images of size $X \times Y$, respectively; n is an additive noise; h is called a point spread function (PSF) of the blur; and subscript i denotes a parameter for the i-th capturing process. In the practical cases, the blurred images may not align due to relative translation or rotation. The pure translation can be included as a shifted versions of the PSFs while image alignment techniques [10], [13], [14] are necessary to correct the alignment for other misalignments before the identification process.

From (1), in the case of noiseless condition, a convolution of the i-th blurred image, g_i, with the j-th PSF, h_j, is equal to a convolution of the j-th blurred image, g_j, with the i-th PSF, h_i. Accordingly, a cross convolution relation between any pair of blurred images can be obtained as

$$h_j * (g_i - n_i) = h_i * \left(g_j - n_j\right). \tag{2}$$

However, due to the noise, the PSFs which satisfy the equality in (2) may not be obtained in the practical situations. In that case, a cross comparison error is evaluated by

$$\xi_{ji}(q, r) = q * (g_i - n_i) - r * \left(g_j - n_j\right), \tag{3}$$

where ξ_{ji} is the cross comparison error between a pair of the j-th and the i-th blurred images; q and r are estimated blur PSFs for the j-th and the i-th capturing process, respectively. From (1) and (3), $\xi_{ji}(q, r)$ becomes zero when $(q, r) = (h_j, h_i)$. In general, a set of identified PSFs, $\{\hat{h}_i\}_{i=0}^{M-1}$ where M is the number of the capturing process, should be a set of PSFs that minimize a total power of the error function in (3) for every i and j. However, it is not easy to directly solve the minimization problem since there is a number of variables needed for all PSF coefficients and the solution may not be unique depended on the prepared PSF regions. In addition, this minimization problem is also difficult to be solved in the frequency domain.

If one of the PSF, h_i, is given, another PSF, h_j, can be easily obtained from

$$h_j = (g_i - n_i)^{-1} * h_i * \left(g_j - n_j\right). \tag{4}$$

In order to assume that condition, the proposed scheme uses the single-image-based identification algorithm [4] for an initial identification of one PSF which seems to have the least difficulty to identify. A blur identification difficulty is proposed to rank an identification order of a provided set of blurred images, $\{g_i\}_{i=0}^{M-1}$. The PSF of the easiest image which tends to need the least information for identification should be firstly estimated. Then, other blur PSFs can be identified based on (4). Details of the ranking process and initial identification are presented in Sect. 2.1 and Sect. 2.2, respectively. After the initial PSFs are identified, an iterative feedback scheme in Sect. 2.3 is applied for a further improvement. A flow diagram for the proposed identification stage is shown in Fig. 1.

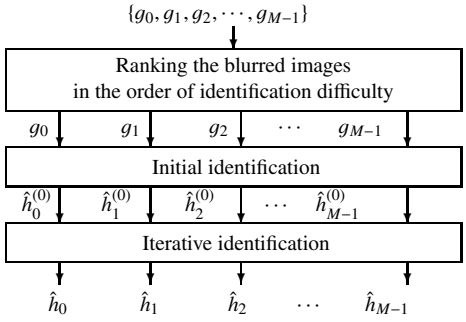

Fig. 1 Proposed three-stage identification scheme.

2.1 Ranking the Difficulty of Blur Identification

The first step of the proposed identification scheme is to rank blurred images according to the difficulty of identification. The blur identification difficulty is introduced to evaluate the difficulty to identify the PSF from the blurred image which includes a confidence level of identified blur parameters by using a single image. The identification difficulty can be determined by considering a size and a shape of support region for PSF coefficients. For the cases of two linear motion blurs, since the motion length corresponds to the number of unknowns, a blur with longer motion length tends to have more difficulty to identify than a blur with shorter motion length. In addition, non-linear motion blurs tends to have more difficulty to identify than linear motion blurs with the same total motion length. Finally, for a comparison of two non-linear motion blurs, a piecewise linear approximation is used. The identification difficulty can be compared by counting the number of piecewise linear motion components. The non-linear motion blur which has more piecewise linear components tends to have more difficulty to identify than others with the same total motion lengths.

To find the identification difficulty, motion directional components are firstly analyzed based on the piecewise linear motion model. Then, the motion length corresponding to each direction is estimated. As a result, the support number of PSF coefficients can be obtained. Section 2.1.1 and Sect. 2.1.2 give brief reviews of the proposed algorithms to analyze the motion directions and lengths in the piecewise

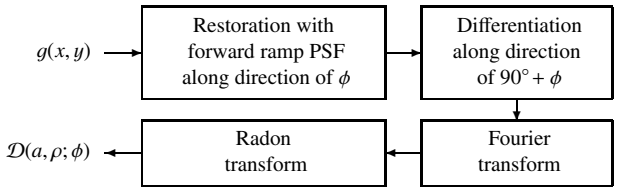

Fig. 2 Motion direction analysis function.

linear model which have been introduced for the single-image-based identification in our prior work [4]. By using the information from the motion direction and length analysis processes, the blur identification difficulty can be evaluated. A mathematical expression for the blur identification difficulty is described in Sect. 2.1.3. After the identification difficulty has been evaluated for every blurred image, the set of provided blurred images is ranked in an ascending order of the identification difficulty. The ordered set of blurred images is represented by $[g_0, g_1, \ldots, g_{M-1}]$ where g_0 and g_{M-1} are the blurred images with the lowest and the highest identification difficulties, respectively.

2.1.1 Analysis of Directional Components

To analyze the directional components of the motion blur for each blurred image, a motion direction analysis function, $\mathcal{D}$, is defined as shown in Fig. 2. Firstly, to stimulate and strengthen strips along the blur direction, each blurred image is restored on trial by assuming the linear motion blur along a trial direction of ϕ and supposing that the distribution of PSF coefficients are forward ramp [3], [4]. Then, it is differentiated along the direction of $90° + \phi$. A Fourier transform is applied to each image derivative to observe the motion directions from a spectrum characteristic. Finally, a Radon transform is employed in frequency domain, resulting in the motion direction analysis function, $\mathcal{D}(a, \rho; \phi)$, where a and ρ represent the dimensions of an angle and a distance from the origin, respectively.

The motion directions are corresponding to the dominant angles in $\mathcal{D}$. In order to locate the dominant angles, local maxima are emphasized by using a high-pass filtering operator as

$$\tilde{\mathcal{D}}(a; \phi) = \bar{\mathcal{D}}(a; \phi) - \frac{1}{2A} \int_{-A}^{A} \bar{\mathcal{D}}(a; \phi) da, \tag{5}$$

$$\text{where } \bar{\mathcal{D}}(a; \phi) = \frac{1}{2P} \int_{-P}^{P} \mathcal{D}(a, \rho; \phi) d\rho, \tag{6}$$

A and P are adjusting parameters for the filter, and $\tilde{\mathcal{D}}$ is a peak emphasized direction analysis function. Since, in the practical cases, the identified motion directions are possible to be lost near the direction of $90° + \phi$ due to the differentiation process, a scheme which uses multiple trial motion direction is preferable. As a result, the motion directional components can be obtained by applying the following iterative scheme.

Initialization: An initially identified set of motion directions denoted by $\{\hat{\theta}_i^{(0)}\}_{i=1}^{\hat{C}^{(0)}}$ can be obtained from a set of locations of local maxima of $\Psi^{(0)}(a) = \max(\tilde{\mathcal{D}}(a; 0°), \tilde{\mathcal{D}}(a; 90°))$ whose values are over a pre-determined threshold. As a result, the number of the initial identified motion components, $\hat{C}^{(0)}$, is equal to the number of local maxima of $\Psi^{(0)}(a)$ whose values are over the threshold.

Updating: The identified set of motion directions in the k-th iteration, $\{\hat{\theta}_i^{(k)}\}_{i=1}^{\hat{C}^{(k)}}$, is the set of locations of local maxima of $\Psi^{(k)}(a)$ whose values are over a threshold where

$$\Psi^{(k)}(a) = \max_i \begin{pmatrix} \Psi^{(k-1)}(a), \tilde{\mathcal{D}}(a; \hat{\theta}_i^{(k-1)}), \\ \tilde{\mathcal{D}}(a; 90° + \hat{\theta}_i^{(k-1)}) \end{pmatrix}, \tag{7}$$

and $\hat{C}^{(k)}$ is the number of identified motion components in the k-th iteration which is obtained from the number of local maxima of $\Psi^{(k)}(a)$ whose values are over the threshold. The iteration can be terminated when a change of the identified results is small enough. In the end of this step, a set of identified motion directions, $\{\hat{\theta}_i\}_{i=1}^{\hat{C}}$, and an estimated number of motion components, $\hat{C}$, are obtained for each blurred image.

The number of the identified motion components depends on the threshold level. The threshold level can be empirically chosen based on experiments or experiences [4] while another solution for selecting the threshold can be described by a probability function. The probability that the direction a is the correct blur direction of the given blurred image g can be defined by

$$P(a|g) = \begin{cases} e^{-\left|\frac{\bar{\Psi}}{\Psi(a)-\bar{\Psi}}\right|}; & \Psi(a) > \bar{\Psi}, \\ 0; & \Psi(a) \le \bar{\Psi}, \end{cases} \tag{8}$$

where $\bar{\Psi} = \frac{1}{\pi} \int_0^{\pi} \Psi(a) da$ is the mean of Ψ. From (8), the probability function is described by $\Psi(a)$. The higher $\Psi(a)$ compared to the mean $\bar{\Psi}$, the higher possibility that a is the actual blur direction. Now, suppose that all actual directions of motion approximately locate in the locations of local maxima. In other words, they are members of $\mathcal{A} = \{\dot{a}_i\}$ where $\dot{a}_i$ is a location of each local maximum of $\Psi(a)$ which is a candidate of the motion blur directions. A selection kernel denoted by $\mathcal{B} = \{b_i\}$ is a set of binary values where the direction $\dot{a}_i$ is selected as the identifed motion direction if $b_i = 1$ and the direction $\dot{a}_i$ is discarded if $b_i = 0$. The possibility that the selection kernel $\mathcal{B}$ yields the correct set of motion direction for the given g and $\mathcal{A}$ can be obtained as

$$P(\mathcal{B}|g, \mathcal{A}) = \prod_i |P(\dot{a}_i|g) - b_i| \,. \tag{9}$$

To maximize the probability function in (9),

$$b_i = \begin{cases} 1; & P(\dot{a}_i|g) \ge 1 - P(\dot{a}_i|g), \\ 0; & P(\dot{a}_i|g) < 1 - P(\dot{a}_i|g). \end{cases} \tag{10}$$

From (10), the direction $\dot{a}_i$ is selected as the motion direction ($b_i = 1$) when $P(\dot{a}_i|g) \geqslant 0.5$ or $\Psi(\dot{a}_i) \geqslant \left(1 + \frac{1}{\ln(2)}\right)\bar{\Psi}$. As a result, based on the maximization of the probability function in (8), the threshold level can be set to 2.4427 times of the mean of $\Psi(a)$.

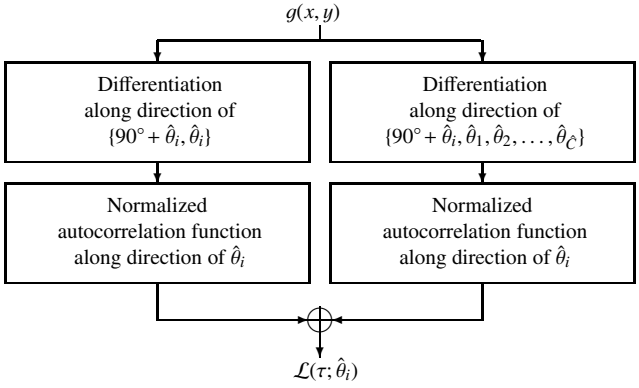

Fig. 3 Motion length analysis function.

2.1.2 Estimation of Motion Length

For each blurred image, a motion length analysis function, $\mathcal{L}$, is computed as shown in Fig. 3. In order to estimate the motion length, $\hat{L}_i$, corresponding to every identified direction of $\hat{\theta}_i \epsilon \{\hat{\theta}_1, \hat{\theta}_2, \ldots, \hat{\theta}_{\hat{C}}\}$, the blurred image derivatives along both directions of $90° + \hat{\theta}_i$, and $\hat{\theta}_i$ are continuously computed. In parallel, the image differentiation along every direction of $90° + \hat{\theta}_i, \hat{\theta}_1, \hat{\theta}_2, \ldots$, and $\hat{\theta}_{\hat{C}}$ are continuously applied to the blurred image to reduce the effect from the other directional components. Then, the normalized autocorrelation functions along the direction of $\hat{\theta}_i$ are computed to both image derivatives. After that, the length analysis function, $\mathcal{L}(\tau; \hat{\theta}_i)$, can be obtained by a summation of two normalized autocorrelation functions where τ represents a lag in the autocorrelation function along the direction of $\hat{\theta}_i$. Finally, the motion length $\hat{L}_i$ can be estimated from a location of the global minima of $\mathcal{L}(\tau; \hat{\theta}_i)$. After the process has been repeated for every direction of $\{\hat{\theta}_i\}_{i=1}^{\hat{C}}$, a set of identified motion components in the piecewise linear model, $\{(\hat{\theta}_i, \hat{L}_i)\}_{i=1}^{\hat{C}}$, for each blurred image is obtained in the end of this stage.

2.1.3 Blur Identification Difficulty

Based on the information obtained from the motion directions and lengths analysis processes, the blur identification difficulty can be determined by the number of necessary support PSF coefficients and the confidence level of identification by using the single-image-based approaches. The blur identification difficulty, γ, is defined by the three parts as

$$\gamma = \gamma_S \gamma_D \gamma_L. \tag{11}$$

In (11), γ_S corresponds to a size of area of support region for PSF coefficients which is defined by

$$\gamma_S = \hat{C} \sum_{i=1}^{\hat{C}} \hat{L}_i. \tag{12}$$

From (12), the identification difficulty increases due to the total motion length and the number of piecewise components which correspond to the number of variable and a level of non-linearity, respectively. Higher γ_S means that there are more variables to identify the corresponding PSF or blur identification is more difficult.

γ_D corresponds to the identification difficulty in consideration of a confidence level of the estimated motion directions. Since the motion directions are identified by using the locations of local maxima in the direction analysis function, $\Psi(a)$, a higher peak increases the confidence level of identification or reduces the identification difficulty. Consequently, γ_D is defined by the ratio of the height of the local maxima of the direction analysis function, $\Psi(\hat{\theta}_i)$, to the mean level as

$$\gamma_D = \sum_{i=1}^{\hat{C}} \left| \frac{\bar{\Psi}}{\Psi(\hat{\theta}_i) - \bar{\Psi}} \right|. \tag{13}$$

Higher γ_D corresponds to lower confidence level of the estimation or identification is more difficult.

On the other hand, γ_L corresponds to the identification difficulty in consideration of a confidence level of the estimated motion lengths. In a similar way to γ_D, the motion length is identified by using the location of global minima of the length analysis function, $\mathcal{L}$. The depth of global minima increases the confidence level of identification or reduces the identification difficulty. γ_L is defined by the ratio of the depth of global minima $\mathcal{L}(\hat{L}_i; \hat{\theta}_i)$ to the depth the second lowest local minima, $\mathcal{L}_{2\min}(\hat{\theta}_i)$, as

$$\gamma_L = \sum_{i=1}^{\hat{C}} \left| \frac{\mathcal{L}_{2\min}(\hat{\theta}_i)}{\mathcal{L}(\hat{L}_i; \hat{\theta}_i) - \mathcal{L}_{2\min}(\hat{\theta}_i)} \right|. \tag{14}$$

Higher γ_L means lower confidence level of the length estimation or higher identification difficulty.

After the motion directions and lengths are analyzed and the identification difficulties are evaluated for every blurred image, the set of blurred images can be ranked in an ascending order of the identification difficulty, resulting in $[g_0, g_1, \ldots, g_{M-1}]$.

2.2 Initial Identification Stage

From the ordered set of the blurred image, the identification can be started from the blurred image g_0 that seems to have the easiest PSF to identify. The PSF h_0 is initially identified by using only g_0 via the single-image-based identification method. The initial estimation of h_0 is denoted by $\hat{h}_0^{(0)}$. In this work, h_0 is initially approximated by the model of constant velocity or uniform distribution of PSF while the motion route is identified by using our prior work on the single-image-based identification scheme [4]. The motion route can be approximately estimated in the piecewise linear model by using the directional and motion length analysis functions that are presented in Sect. 2.1.1 and Sect. 2.1.2. (Note that the piecewise linear model is only used for the initial guess of the identification process while the final identified results can be converted to the actual blur PSFs which

can be any type of the shift-invariant motion blurs.)

Next, the multiple-image-based identification approach is started from estimation of h_1 to h_{M-1}, respectively. The PSFs are identified in the ascending order of the identification difficulty where h_j can be estimated by using h_i for $i < j$ based on minimization of the total error power of the error function in (3). The initial estimation of h_j is denoted by $\hat{h}_j^{(0)}$. Consequently, the PSFs which have more difficulty are estimated by using more blurred images with the initial identified PSFs that provide more information.

For the error minimization, the cross comparison error in (3) can be re-written in the matrix and vector form as

$$\boldsymbol{\xi}_{ji}(\mathbf{q},\mathbf{r}) = (\mathbf{G}_i - \mathbf{N}_i)\,\mathbf{q} - \left(\mathbf{G}_j - \mathbf{N}_j\right)\mathbf{r}, \tag{15}$$

where $\boldsymbol{\xi}_{ji}$, $\mathbf{q}$, and $\mathbf{r}$ are XY-element vector representation of $\xi_{ji}(x,y)$, $q(x,y)$, and $r(x,y)$, respectively; and $\mathbf{G}_i$, $\mathbf{G}_j$, $\mathbf{N}_i$, and $\mathbf{N}_j$ are $XY \times XY$ matrix operators corresponding to the convolution with $g_i(x,y)$, $g_j(x,y)$, $n_i(x,y)$, and $n_j(x,y)$, respectively. To minimize the cross comparison errors between a current PSF estimate, $\hat{\mathbf{h}}_j^{(0)}$, and every estimated PSF, $\{\hat{\mathbf{h}}_i^{(0)}\}_{i=0}^{j-1}$, a raw estimation of $\mathbf{h}_j$ is defined by

$$\tilde{\mathbf{h}}_j^{(0)} = \arg\min_{\mathbf{q}} E\left\{\sum_{i=0}^{j-1}\left\|\boldsymbol{\xi}_{ji}(\mathbf{q},\hat{\mathbf{h}}_i^{(0)})\right\|_2^2\right\}, \tag{16}$$

where $\tilde{\mathbf{h}}_j^{(0)}$ denotes the raw estimation of $h_j(x,y)$ in vector form; and $\hat{\mathbf{h}}_i^{(0)}$ is a vector form of $\hat{h}_i^{(0)}(x,y)$. In the end of the identification process, a post-processing process is employed to condition the raw estimation, $\tilde{\mathbf{h}}_j^{(0)}$, to obtain the final result, $\hat{\mathbf{h}}_i^{(0)}$. According to (16), $\tilde{\mathbf{h}}_j^{(0)}$ can be obtained from $\mathbf{q}$ where

$$\frac{\partial E\left\{\sum_{i=0}^{j-1}\left\|\boldsymbol{\xi}_{ji}(\mathbf{q},\hat{\mathbf{h}}_i^{(0)})\right\|_2^2\right\}}{\partial \mathbf{q}} = 0, \tag{17}$$

resulting in

$$\tilde{\mathbf{h}}_j^{(0)} = \left[\sum_{i=0}^{j-1}\left(\mathbf{G}_i^T\mathbf{G}_i - XY\sigma_i^2\mathbf{I}\right)\right]^{-1}\sum_{i=0}^{j-1}\mathbf{G}_i^T\hat{\mathbf{G}}_j\hat{\mathbf{h}}_i^{(0)}, \tag{18}$$

where σ_i^2 is a variance of n_i. For implementation, (18) can be written in the frequency domain as

$$\tilde{H}_j^{(0)}(\omega) = \frac{\sum_{i=0}^{j-1} G_i^*(\omega)G_j(\omega)\hat{H}_i^{(0)}(\omega)}{\sum_{i=0}^{j-1}\left[G_i^*(\omega)G_i(\omega) - \sigma_i^2\right]}. \tag{19}$$

By using the frequency domain approach, the number of support coefficients for the raw estimation of PSF, $\tilde{h}_j(x,y)$, can be ideally unlimited; therefore, the initial identification of the support region is unnecessary and, roughly, the computational cost does not increase by the size of support region. However, the identification errors may appear in the redundant positions.

As a result, after the raw estimation, $\tilde{h}_j(x,y)$, is obtained, a post-processing described in the following steps is applied for conditioning the results based on the characteristic of motion blur.

Step 1: Based on an assumption that the large values appearing in the raw estimation, $\tilde{h}_j(x,y)$, should be included in the identified PSF, $\hat{h}_j(x,y)$, (small values may be dominated by errors) the locations of PSF coefficients whose values are over than a threshold level denoted by T is marked. A set of marked positions is denoted by $\mathcal{M}_j$ where $\mathcal{M}_j = \{(x,y)|\tilde{h}_j(x,y) \geq T\}$. T can be decided based on the estimated number of PSF coefficients which corresponds to the total motion length, $\sum_{i=1}^{\hat{C}}\hat{L}_i$, including with margin due to an error tolerance of the identified motion lengths and spread of the coefficients due to a quantization of non-integer pixels' index in a discrete spatial domain. T can be assigned to obtain the desired number of non-zero coefficients in $\hat{h}_j(x,y)$.

Step 2: Since the motion blur should be characterized by a one connected component, a connected component labeling algorithm [15] is applied to $\mathcal{M}_j$. In consideration of the number of members of every connected component, positions of undesired components are removed from $\mathcal{M}_j$ if the number of their connected members is too small. On the other hand, if any pair of connected components are very close to each other, positions in a gap between two connected components are filled in $\mathcal{M}_j$.

Step 3: Normalization is applied to satisfy an energy conservation constraint, $\sum_{x,y}\hat{h}_j(x,y) = 1$. Finally, the identified PSF, $\hat{h}_j(x,y)$, can be obtained by,

$$\hat{h}_j(x,y) = \begin{cases} \frac{\tilde{h}_j(x,y)}{\sum_{(x,y)\epsilon\mathcal{M}_j}\tilde{h}_j(x,y)}; & (x,y)\epsilon\mathcal{M}_j, \\ 0; & \text{otherwise.} \end{cases} \tag{20}$$

2.3 Iterative Identification Stage

From the initial identification stage, the set of initial identified PSFs, $\{\hat{\mathbf{h}}_i^{(0)}\}_{i=0}^{M-1}$, is now obtained. In this section, the iterative algorithm is applied for more improvement because more information is now provided. The identified PSFs can be updated to obtain the better results by feeding back previous versions of estimated PSFs. The proposed iterative algorithm tries to minimize the cross comparison errors between the current updating blur PSF, $\hat{\mathbf{h}}_j^{(k)}$, and other estimated PSFs which are obtained in the previous iteration, $\{\hat{\mathbf{h}}_i^{(k-1)}\}_{i=j+1}^{M-1}$, or has been updated in the current iteration, $\{\hat{\mathbf{h}}_i^{(k)}\}_{i=0}^{j-1}$. Consequently, the raw estimation of h_j in the k-th iteration can be written as

$$\tilde{\mathbf{h}}_j^{(k)} = \arg\min_{\mathbf{q}} E\left\{\begin{array}{l}\sum_{i=0}^{j-1}\left\|\boldsymbol{\xi}_{ji}(\mathbf{q},\hat{\mathbf{h}}_i^{(k)})\right\|_2^2 \\ +\sum_{i=j+1}^{M-1}\left\|\boldsymbol{\xi}_{ji}(\mathbf{q},\hat{\mathbf{h}}_i^{(k-1)})\right\|_2^2\end{array}\right\}. \tag{21}$$

$\tilde{\mathbf{h}}_j^{(k)}$ which satisfies (21) can be obtained in the frequency domain as

$$\tilde{H}_j^{(k)}(\omega) = \frac{\sum_{i=0}^{j-1} G_i^* G_j \hat{H}_i^{(k)} + \sum_{i=j+1}^{M-1} G_i^* G_j \hat{H}_i^{(k-1)}}{\sum_{i=0, i\neq j}^{M-1} \left[G_i^* G_i - \sigma_i^2\right]}. \quad (22)$$

After the raw estimation is obtained, the same post conditioning processes described in 2.2 is employed to obtain the final estimated blur PSF, $\hat{\mathbf{h}}_j^{(k)}$. Finally, the iteration is terminated when the difference of updated PSFs, $\sum_{j=0}^{M-1} \|\hat{\mathbf{h}}_j^{(k)} - \hat{\mathbf{h}}_j^{(k-1)}\|_2^2$, is small enough.

3. Iterative Deconvolution Scheme Based on Regional Optimal Termination

In this work, a modified version of Landweber iterative deconvolution scheme [12] is employed. The proposed spatial adaptive scheme can be written in the matrix and vector form as

$$\hat{\mathbf{f}}_j^{(k)} = \hat{\mathbf{f}}_j^{(k-1)} + \frac{\beta \mathbf{W}_j^{(k-1)}}{M-1} \sum_{i=0, i\neq j}^{M-1} \hat{\mathbf{H}}_i^T \left(\mathbf{g}_i - \hat{\mathbf{H}}_i \hat{\mathbf{f}}_j^{(k-1)}\right), \quad (23)$$

$$\text{where } \hat{\mathbf{f}}_j^{(0)} = \frac{1}{M-1} \sum_{i=0, i\neq j}^{M-1} \mathbf{g}_i, \quad (24)$$

$\mathbf{W}_j$ is a weighting matrix operator, β is a step size, and superscript (k) denotes the iteration round. The restored images, $\hat{\mathbf{f}}_j^{(k)}$, are combined together to obtain the final result as

$$\hat{\mathbf{f}}^{(k)} = \frac{1}{M} \sum_{j=0}^{M-1} \hat{\mathbf{f}}_j^{(k)}, \quad (25)$$

where $\hat{\mathbf{f}}^{(k)}$ represents the final restored result in the vector form. From (23), the proposed scheme includes two modifications from the conventional Landweber method. The first modification is the weighting matrix operator $\mathbf{W}_j$ for spatial adaptation. The other modification is an inequality condition $i \neq j$ in the summation. According to (23) and (1), $\hat{\mathbf{f}}_j^{(k)}$ and $\mathbf{n}_j$ are uncorrelated because $\hat{\mathbf{f}}_j^{(k)}$ is obtained from g_i where $i \neq j$. This uncorrelated property will be applied to increase the accuracy of an error analysis for an estimation of optimal terminating points. However, to avoid the ill-posed problem which may appear in (23) when $M \leq 2$, the deconvolution process is modified to

$$\hat{\mathbf{f}}^{(k)} = \hat{\mathbf{f}}_j^{(k)} = \hat{\mathbf{f}}_j^{(k-1)} + \frac{\beta \mathbf{W}_j^{(k-1)}}{M} \sum_{i=0}^{M-1} \hat{\mathbf{H}}_i^T \left(\mathbf{g}_i - \hat{\mathbf{H}}_i \hat{\mathbf{f}}_j^{(k-1)}\right), \quad (26)$$

$$\text{where } \hat{\mathbf{f}}_j^{(0)} = \frac{1}{M} \sum_{i=0}^{M-1} \mathbf{g}_i. \quad (27)$$

To evaluate the result, a restoration error, $e(x, y)$, is defined as

$$e^{(k)}(x, y) = f(x, y) - \hat{f}^{(k)}(x, y) = \frac{1}{M} \sum_{j=0}^{M-1} e_j^{(k)}(x, y), \quad (28)$$

$$\text{where } e_j^{(k)}(x, y) = f(x, y) - \hat{f}_j^{(k)}(x, y). \quad (29)$$

Typically, there is a trade-off between residual blur and amplified noise components in the restoration process. The deblurring operator which reduces blur component by amplifying lost high frequency components may also enlarge the noise. In consideration of the smoothness of the images, the weighting operator, $w_j^{(k)}(x, y)$, is applied to suppress the noise amplification in smooth regions where degradation is dominated by the noise and sharpen the image in non-smooth regions where the error is dominated by the blur component. Accordingly, in the homogeneous regions, $w_j^{(k)}$ should be small to slow down the noise magnification rate. On the contrary, $w_j^{(k)}$ could be higher in the edgy regions to accelerate the blur reduction rate. As a results, the proposed scheme in (23) starts from $w_j^{(0)}(x, y) = 1$ for all (x, y). Then, $w_j^{(k)}(x, y)$ is set to zero to stop the iteration in order to obtain the optimal result which is analyzed by decomposing the image into sub-regions and considering their estimated mean square restoration error. The details are described in the following steps.

Region Decomposition : In consideration of the blur component, $\Delta(x, y)$, which is a difference between the original and its blurred version,

$$\Delta(x, y) = \frac{1}{M} \sum_{j=0}^{M-1} \left(\hat{h}_j * f(x, y) - f(x, y)\right)^2, \quad (30)$$

the image is decomposed into regions of $\{\mathcal{R}_i\}_{i=1}^{\alpha}$ where α is the number of decomposed regions which can determined by the size of image. The restoration should be early terminated to suppress the noise amplification in the area where $\Delta(x, y)$ is small since there is less blur component to be restored. On the other hand, the restoration should be late terminated to reduce the blur component if $\Delta(x, y)$ is high. Since f is unknown, Δ can not be obtained from (30). An approximation, $\hat{\Delta}$, is found by using the blurred images as

$$\hat{\Delta}(x, y) = \frac{1}{M^2} \sum_{j=0}^{M-1} \sum_{i=0}^{M-1} \left(\hat{h}_j * g_i(x, y) - g_i(x, y)\right)^2. \quad (31)$$

Then, in this work, $\mathcal{R}_1$ which corresponds to the set of pixels in the smoothest region can be obtained from the pixels (x, y) whose values of $\hat{\Delta}$ are less than the 50th percentile; $\mathcal{R}_i$ corresponds to the set of pixels where $\hat{\Delta}$ is in between the $100(1-2^{-i+1})$-th percentile and the $100(1-2^{-i})$-th percentile; and $\mathcal{R}_\alpha$ corresponds to the set of pixels in the most edgy region whose values of $\hat{\Delta}$ are larger than the $100(1-2^{-\alpha+1})$-th percentile. In this stage, median filters may be employed to the decomposed region to remove impulsive enclaves.

Stopping Rule: Ideally, the restoration should be stopped to hold the best result by setting $w_j^{(k)}(x, y)$ to zero when the result does not improve or $|e_j^{(k)}(x, y)| -$

$|e_j^{(k+1)}(x,y)| \leq 0$. However, $e_j^{(k)}$ can not practically be obtained from (29) because f is unknown. As a result, in order to evaluate the restoration result, a discrepancy error, $\varepsilon_j(x,y)$, is defined by

$$\varepsilon_j^{(k)}(x,y) = g_j(x,y) - \hat{h}_j * \hat{f}_j^{(k)}(x,y). \tag{32}$$

From (29) and (32), by assuming that the identified PSF is approximately equal to the original PSF or $\hat{h}_j \approx h_j$, the relation between $e_j^{(k)}$ and $\varepsilon_j^{(k)}$ can be approximated by

$$\varepsilon_j^{(k)}(x,y) \approx \hat{h}_j * e_j^{(k)}(x,y) + n_j(x,y). \tag{33}$$

Now the error analysis is separately considered into two cases according to the number of blurred images, M.

In the case of $M \geq 3$, since e_j is a function of $\hat{f}_j$ which is uncorrelated to n_j according to (29) and (23),

$$E\left\{\left|\varepsilon_j^{(k)}(x,y)\right|^2\right\} \approx E\left\{\left|\hat{h}_j * e_j^{(k)}(x,y)\right|^2\right\} + \sigma_j^2. \tag{34}$$

$\sum_{x,y}(|e_j^{(k)}|^2 - |e_j^{(k+1)}|^2)$ is assumed to have the same sign with $\sum_{x,y}(|h_j * e_j^{(k)}|^2 - |h_j * e_j^{(k+1)}|^2)$ when the size of summation area of (x,y) is large enough. Finally, $w_j^{(k)}(x,y)$ for $(x,y) \in \mathcal{R}_i$ when $i = 1, 2, \ldots, \alpha$ is set to zero when

$$\sum_{(x,y)\in\mathcal{R}_i}\left(\left|\varepsilon_j^{(k)}(x,y)\right|^2 - \left|\varepsilon_j^{(k+1)}(x,y)\right|^2\right) \leq 0. \tag{35}$$

On the other hand, when $M \leq 2$, since the correlation between e_j and n_j can not be neglected, the error analysis becomes more complicated. In this work, the conventional stopping rule [11], [12] is used. Thus, $w^{(k)}(x,y)$ for $(x,y) \in \mathcal{R}_i$ and $M \leq 2$ is set to zero when there is a small improvement of the discrepancy error,

$$\sum_{(x,y)\in\mathcal{R}_i}\sum_{j=0}^{M-1}\left(\left|\varepsilon_j^{(k)}(x,y)\right|^2 - \left|\varepsilon_j^{(k+1)}(x,y)\right|^2\right). \tag{36}$$

Unfortunately, when $M \geq 3$, the proposed deconvolution scheme increases a computational cost $M-1$ times comparing to the conventional multiple-images-based schemes [10] and M^2-M times comparing to the conventional single-images-based schemes [12].

4. Experimental Results

In this section, the performance of the proposed method is demonstrated by simulation and real world examples in Sect. 4.1 and Sect. 4.2, respectively. The proposed method was used to reconstruct the original scene from various sets of motion blurred images. In the deconvolution step, the images are decomposed into three sub-regions ($\alpha = 3$) based on the proposed scheme for all experiments. For every simulation, Gaussian noises were added to the blurred images, resulting in $SNR = 30$ dB. The quality of the images (degraded and restored images) in the simulation are evaluated by using *PSNR*. For $s(x,y) = g_i(x,y)$ or $\hat{f}(x,y)$,

$$PSNR_s = 10\log\left[\frac{255^2XY}{\sum_{x,y}(s(x,y) - f(x,y))^2}\right]. \tag{37}$$

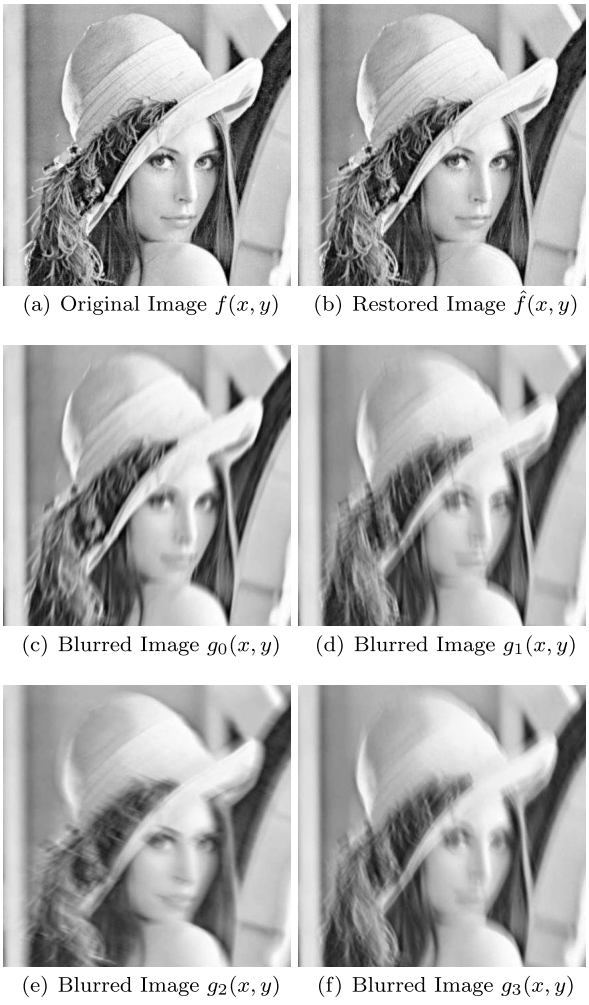

(a) Original Image $f(x,y)$ (b) Restored Image $\hat{f}(x,y)$

(c) Blurred Image $g_0(x,y)$ (d) Blurred Image $g_1(x,y)$

(e) Blurred Image $g_2(x,y)$ (f) Blurred Image $g_3(x,y)$

Fig. 4 Original, blurred and restored versions of LENNA image (cropped from the original size for displaying.) (a) Original image. (b) Restored image. (c)–(f) Input blurred images.

4.1 Simulated Blur

Experiment I: In this example, the proposed scheme was tested to restore the LENNA image from four simulated motion blurred versions. The original LENNA image of size 512×512 shown in Fig. 4(a) was blurred by four simulated PSFs in Figs. 5(a)–(d). The corresponding degraded images are shown in Figs. 4(c)–(f).

In the first step of blur identification, the identification difficulties of four blurred images are evaluated, resulting in Table 1. g_0 is the blurred image with the lowest identification difficulty that consists of only one linear motion component and has the shortest motion length. On the other hand, g_3 which is composed of three estimated components obtains the highest identification difficulty. After the blurred images are ranked, the blur PSFs are identified according to the proposed algorithm. The identified PSFs are illustrated in Figs. 5(e)–(h). It is clear that the identified results are similar to the original PSFs in Figs. 5(a)–(d). Then, the orig-

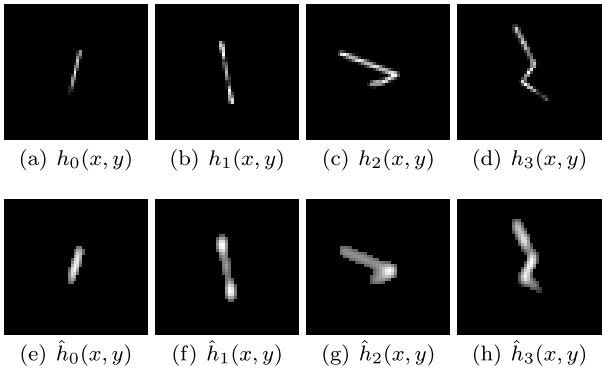

(a) $h_0(x, y)$ (b) $h_1(x, y)$ (c) $h_2(x, y)$ (d) $h_3(x, y)$

(e) $\hat{h}_0(x, y)$ (f) $\hat{h}_1(x, y)$ (g) $\hat{h}_2(x, y)$ (h) $\hat{h}_3(x, y)$

Fig. 5 Original and identified blur PSFs of Figs. 4(c)–(f) (displaying size is 49×47.) (a)–(d) Original simulated PSFs of Figs. 4(c)–(f), respectivly. (e)–(h) Identified PSFs of Figs. 4(c)–(f), respectively, by Proposed algorithm.

Table 1 Blur identification difficulty of Figs. 4(c)–(f).

Blurred Image	*PSNR* [dB]	Set of Identified Motion Components $(\hat{\theta}_i, \hat{L}_i)$	γ_S	γ_D	γ_L	γ
g_0	25.7928	$(73°, 13)$	13	0.099	0.112	0.14
g_1	21.6137	$(100°, 22)$	22	0.102	0.199	0.45
g_2	20.4297	$(44°, 10)(156°, 21)$	62	0.475	1.475	43.42
g_3	21.5416	$(56°, 9)(115°, 16)$ $(135°, 8)$	99	1.067	0.557	58.86

inal image is reconstructed by the proposed spatial adaptive scheme. A clear restored result with *PSNR* = 32.34 dB is shown in Fig. 4(b). In addition, the set of the original PSFs showed in Figs. 5(a)–(d) and a set of PSFs that are identified from the single-image-based scheme presented in [4] are also employed to the restoration process in order to compare an effect of the identification results. According to [4], the PSFs are directly modeled by the piecewise linear function corresponding to the identified set of motion components, $(\hat{\theta}_i, \hat{L}_i)$, demonstrated in Table 1 under an assumption of the constant velocity motion. As a result, the restored images with *PSNR* = 34.60 dB and 29.19 dB are obtained when the actual set of PSFs and the PSFs identified by [4] are used for restoration, respectively. It confirms that the proposed identification scheme can improve the results from the single image approach which has less accuracy due to use of information from the only one image.

Experiment II: This experiment is conducted to compare the restoration results of the proposed and conventional methods [4], [8]–[10]. The blurred image g_0 in Fig. 4(c) is restored by the single-image-based scheme [4], the conventional multiple-image-based schemes [8]–[10] and the proposed scheme with an additional image. The comparison of the restoration results are demonstrated in Table 2 via *PSNR*.

The single-image-based scheme [4] provides the lowest *PSNR* = 27.95 dB comparing to other schemes that use two images because both identification and deconvolution steps are operated by using only one blurred image (g_0) which provides the less information comparing to the multiple image cases.

Table 2 Comparison of the restoration results from the proposed scheme and the other schemes.

Restoration Scheme	Provided Set of Images	$PSNR_{\hat{f}}$ [dB]
Proposed Scheme	Two Blurred Images g_0: *PSNR* = 25.79 dB g_1: *PSNR* = 21.61 dB	30.57
Multiple Images with General Blurs [9]	Two Blurred Images g_0: *PSNR* = 25.79 dB g_1: *PSNR* = 21.61 dB	28.75
Two Linear Motion Blurred Images [10]	Two Blurred Images g_0: *PSNR* = 25.79 dB g_1: *PSNR* = 21.61 dB	29.75
Blurred Image and Noisy Image [8]	Blurred Image g_0: *PSNR* = 25.79 dB Noisy Image $f + n$: *SNR* = 3 dB	28.79
Single Blurred Image [4]	Blurred Image g_0: *PSNR* = 25.79 dB	27.95

For [8], the additional shot using short exposure time to avoid the blur is needed. The noisy version of the original image, $f + n$, is simulated, resulting in *SNR* = 3 dB. The blurred image g_0 is identified by using the noisy image $f + n$ and it is deconvoluted by using the single-image-based scheme. The restored image gains *PSNR* = 28.79 dB. Since the additional information is provided in the identification process, More accurate PSF can be estimated comparing to [4].

In the cases of [10] which has been proposed for restoration of two linear motion blurred images with the different blur direction, two linear blurred images (g_0 and g_1 as the additional image) illustrated in Figs. 4(c)–(d) was chosen as the provided blurred images. In this example, the difference of the direction between two PSF is 25°. The restoration result gains *PSNR* = 29.75 dB which is better than [4], [8] because both identification and deconvolution processes are based on information from two blurred images.

When the same set of blurred images (g_0 and g_1) are used as the observed inputs as in the cases of [10], the restoration result with *PSNR* = 28.75 dB is obtained by using the algorithm based on [9] which has been proposed for restoration of the multiple blurred images with general types of blur. The restoration result is worse than [8], [10] because there are more PSF identification errors that can spread into the redundant support region.

By using the same provided blurred images as in the cases of [9], [10] (g_0 and g_1), the proposed methods can provide the best *PSNR* = 30.57 dB among the other schemes.

In the second part of this experiment, in order to demonstrate the robustness of the proposed scheme in the cases that the direction of two linear motion blurs are the same, h_0 in Fig. 5(a) was rotated to obtained the same direction as h_1 in Fig. 5(b). Then, h_1 and the rotated version of h_0 are used as the original PSFs to simulated two blurred blurred versions of LENNA image. From this condition, the restoration result from the proposed methods gains *PSNR* = 30.48 dB while the conventional method [10] which is weak for this condition provides *PSNR* = 25.97 dB.

Table 3 Restoration results from various set of original images and simulated PSFs by using proposed scheme.

Image (512×512)	PSFs (ranked by γ)	$\max_i \left(PSNR_{g_i}\right)$ [dB]	$PSNR_{\hat{f}}$ [dB]
LENNA	$[h_b, h_c]$	25.79	30.57
	$[h_e, h_f, h_h]$	22.58	32.68
	$[h_b, h_c, h_h, h_i]$	25.79	32.34
	$[h_b, h_c, h_f, h_l]$	25.79	32.69
PLANE	$[h_d, h_k]$	22.35	30.58
	$[h_a, h_d]$	22.35	32.65
	$[h_e, h_i, h_j]$	23.39	33.08
	$[h_e, h_g, h_i, h_j]$	23.39	34.00
PEPPERS	$[h_a, h_k]$	24.53	31.46
	$[h_g, h_h, h_l]$	25.52	31.80
	$[h_a, h_g, h_l]$	25.52	31.94
	$[h_d, h_f, h_j, h_k]$	24.66	32.23

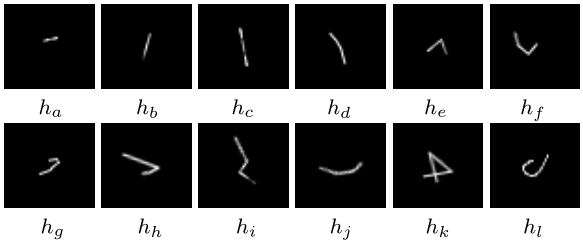

Fig. 6 Original PSFs using for simulating the blur images in Table 2 (Displaying size is 49×47).

Experiment III: In this sub-section, examples of restored results obtained from the proposed scheme are given in Table 3. Three samples of the original images and twelve samples of the PSFs illustrated in Fig. 6 are used. In each row of Table 3, the original image is blurred by using two, three, or four PSFs to obtain the set of provided blurred images. The best *PSNR* among the provided degraded images is shown in the column of $\max_i(PSNR_{g_i})$ and the *PSNR* of the restored images are shown in the column of $PSNR_{\hat{f}}$. From Table 3, the restoration results are satisfactory and tend to improve when more blurred image is provided.

4.2 Real World Blur

Example I: In this example, three real world blurred images in Figs. 7(a)–(c) captured from the same scene were deblurred by the proposed scheme. The misalignment is assumed to be the pure translation; therefore, the identification and restoration processes can be operated without an initial correction of the alignment. Firstly, the identification difficulty was computed, resulting in Table 4. Then, the identified PSFs can be obtained as shown in Figs. 8(a)–(c) corresponding to the blurred images in Figs. 7(a)–(c). In this example, phase differences between the blurred images due to misalignment in translation can be observed. Fortunately, the translation can be included as a phase shift of PSFs. The restoration result is demonstrated in Fig. 7(d). The improvement can be clearly seen from the characters and edges of the restored image comparing to the blurred images. Due to the proposed spatial adaptive scheme, the edges can be enhanced while the noise are suppressed in the smooth regions.

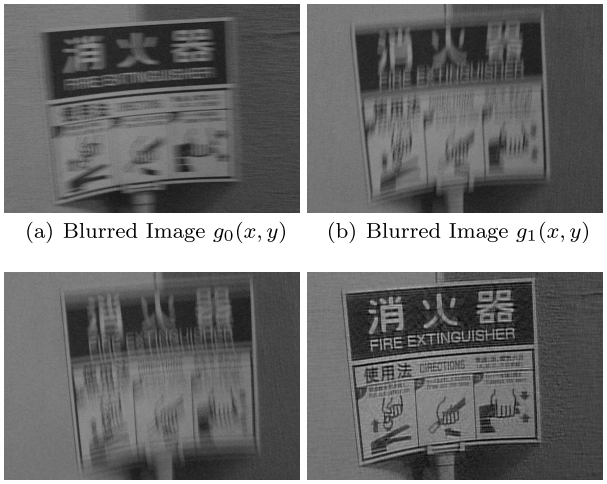

(a) Blurred Image $g_0(x, y)$ (b) Blurred Image $g_1(x, y)$

(c) Blurred Image $g_2(x, y)$ (d) Restored Image $\hat{f}(x, y)$

Fig. 7 Real world blurred images and their restored version of size 620×410 (cropped from the original size 640×480 for displaying.) (a)–(c) Input blurred images. (d) Restored image from given blurred image by using proposed algorithm.

Table 4 Blur identification difficulty of Figs. 7(a)–(c).

Blurred Image	Set of Identified Motion Components $(\hat{\theta}_i, \hat{L}_i)$	γ_S	γ_D	γ_L	γ
g_0	$(4°, 24)$	24	0.045	0.465	0.50
g_1	$(90°, 28)$	28	0.073	2.039	4.17
g_2	$(91°, 18)$	18	0.047	18.136	15.25

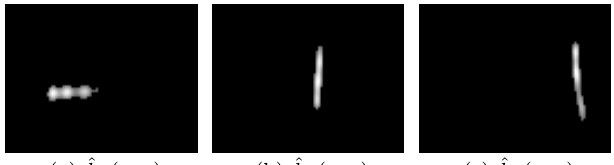

(a) $\hat{h}_0(x, y)$ (b) $\hat{h}_1(x, y)$ (c) $\hat{h}_2(x, y)$

Fig. 8 Identified PSFs of real world blurred images in Figs. 7(a)–(c), respectively (displaying size is 91×71).

Example II: The other example for real world blurred images are demonstrated in Fig. 9. Figures 9(a)–(c) show three blurred images and their corresponding restored result is shown in Fig. 9(d). The identified PSFs for the blurred images in Figs. 9(a)–(c) are illustated in Figs.9(e)–(g), respectively. Since, in this example, the input blurred images have not only large relative translations but also different rotation angles, the image registration process is needed to align the blurred inputs before the identification and restoration processes.

The results obtained from the two examples confirm that the proposed scheme can identify and restore the blurred images with the non-linear motion blurs and non-uniform distribution of PSFs in the real situations.

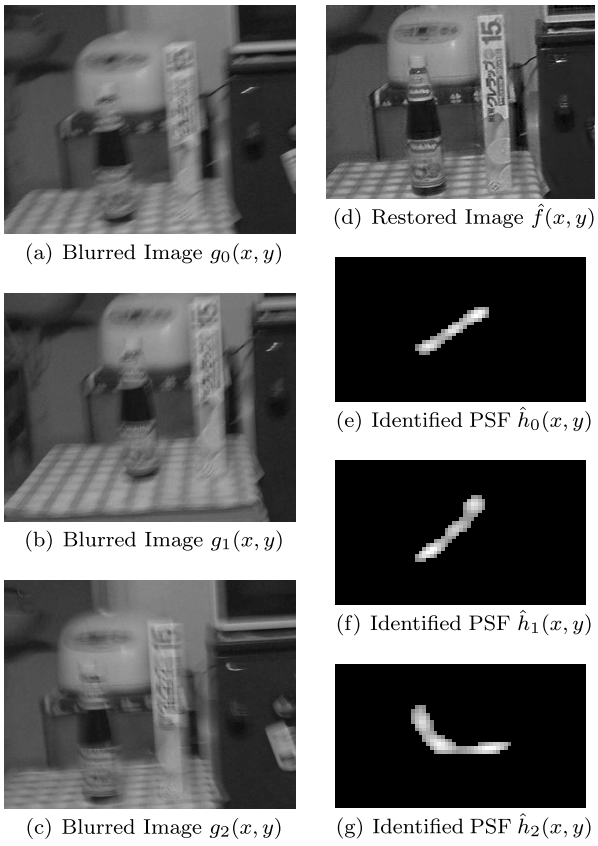

(a) Blurred Image $g_0(x, y)$
(b) Blurred Image $g_1(x, y)$
(c) Blurred Image $g_2(x, y)$
(d) Restored Image $\hat{f}(x, y)$
(e) Identified PSF $\hat{h}_0(x, y)$
(f) Identified PSF $\hat{h}_1(x, y)$
(g) Identified PSF $\hat{h}_2(x, y)$

Fig. 9 The second example of the real world blurred images (a)–(c) input blurred images of size 620×410 (cropped from the original size 640×480 for displaying). (d) Restored image from given blurred images by proposed scheme of size 536×386 (cropped from the original size for displaying). (e)–(g) Corresponding identified PSFs of (a)–(c), respectively (Displaying size is 67×36).

5. Conclusion

The multiple-image-based scheme for restoration of the general motion blur was proposed. The proposed scheme includes both identification and doconvolution algorithms. In the identification step, the identification difficulty was introduced to rank the blurred images for the initial estimation of the PSF which has less difficulty by using the single-image-based approach. By using the initial identified result, the PSFs can iteratively be identified based on the cross convolution relations of the pairs of blurred images. For the doconvolution step, the blurred images are restored by decomposing the image into sub-regions and applying the different optimal terminating point to each region. The experiment demonstrated that the proposed scheme can restore the non-linear motion blurs with non-uniform PSFs via the examples of the simulation and real world blurred images and provides the better restoration results in a comparison with the conventional methods.

References

[1] Y. Yitzhaky and N.S. Kopeika, "Identification of blur parameters from motion blurred images," CVGIP: Graphical models and image processing, vol.59, no.5, pp.321–332, Sept. 1997.
[2] Y. Chen and I. Choa, "An approach to estimating the motion parameters for a linear motion blurred image," IEICE Trans. Inf. & Syst., vol.E83-D, no.7, pp.1601–1603, July 2000.
[3] W. Tan, J. Zhang, G. Rong, and H. Chen, "Identification of motion blur direction based on analysis of intentional restoration errors," 2004 IEEE Inter. Conf. on Networking, Sensing and Control, vol.2, pp.1253–1258, 2004.
[4] K. Patanukhom and A. Nishihara, "Identification of piecewise linear uniform motion blur," IEICE Trans. Fundamentals, vol.E91-A, no.6, pp.1416–1425, June 2008.
[5] D. Huang, N. Fujiyama, and S. Sugimoto, "Blind image identification and restoration for noisy blurred images based on discrete sine transform," IEICE Trans. Inf.& Syst., vol.E86-D, no.4, pp.727–735, April 2003.
[6] M.A.T. Figueriredo and R.D. Nowak, "An EM algorithm for wavelet-based image restoration," IEEE Trans. Image Process., vol.12, no.8, pp.906–916, Aug. 2003.
[7] M. Ben-Ezra and S.K. Nayar, "Motion-based motion deblurring," IEEE Trans. Pattern Anal. Mach. Intell., vol.26, no.6, pp.689–698, June 2004.
[8] M. Tico, M. Trimeche, and M. Vehvilainen, "Motion blur identification based on differently exposed images," IEEE International Conference on Image Processing, 2006, pp.2021–2024, Oct. 2006.
[9] G.B. Giannakis and R.W. Heath, Jr., "Blind identification of multichannel FIR blurs and perfect image restoration," IEEE Trans. Image Process., vol.9, no.11, pp.1877–1896, Nov. 2000.
[10] A. Rav-Acha and S. Peleg, "Two motion-blurred images are better than one," Pattern Regconit. Lett., vol.26, pp.311–317, 2005.
[11] J. Biemond, R.L. Lagendjik, and R.M. Mersereau, "Iterative methods for image deblurring," Proc. IEEE, vol.78, pp.856–883, May 1990.
[12] L. Liang and Y. Xu, "Adaptive landweber method to deblur images," IEEE Trans. Signal Process., vol.10, no.5, pp.129–132, May 2003.
[13] J.R. Bergen, P. Anandan, K.J. Hanna, and R. Hingorani, "Hierarchical model-based motion estimation," Second European Conference on Computer Vision, 1992, pp.237–252, May 1992.
[14] L.G. Brown, "A survey of image registration techniques," ACM Comput. Surv., vol.24, no.4, pp.325–376, Dec. 1992.
[15] F. Chang, C. Chen, and C. Lu, "A linear-time component-labeling algorithm using contour tracing technique," Computer Vision and Image Understanding, vol.93, no.2, pp.206–220, 2004.

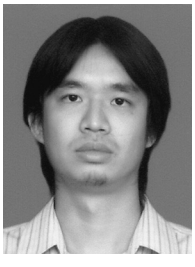

Karn Patanukhom was born in 1981. He received the B.S. and M.S. degrees in Electrical Engineering from Chiang Mai University in 2003 and Tokyo Institute of Technology in 2006, respectively. Since 2006 he has been working toward the Ph.D. degree at the Tokyo Institute of Technology. His research interest is in image processing, especially in image restoration problem.

Akinori Nishihara received the B.E., M.E. and Dr.Eng. degrees in electronics from Tokyo Institute of Technology in 1973, 1975 and 1978, respectively. Since 1978 he has been with Tokyo Institute of Technology, where he is now Professor of the Center for Research and Development of Educational Technology. His main research interests are in one- and multi-dimensional signal processing, and its application to educational technology. He has published more than 200 technical papers in international journals and conferences. He served as an Associate Editor of the IEICE Transactions on Fundamentals of Electronics, Communications and Computer Sciences from 1990 to 1994, and then an Associate Editor of the Transactions of IEICE Part A (in Japanese) from 1994 to 1998. He was an Associate Editor of the IEEE Transactions on Circuits and Systems II from 1996 to 1997 and Editor-in-Chief of Transactions of IEICE Part A (in Japanese) from 1998 to 2000. He served in IEEE Region 10 Executive Committee in various positions, and the Executive Committee of IEEE Tokyo Section and IEEE Japan Council for the last 10 years. He was a member of the Board of Governors, IEEE Circuits and Systems Society (2004–2005), and was Chair of IEEE Circuits and Systems Society Japan Chapter (2006–2007). He was Chair of the IEICE Technical Group on Circuits and Systems from 1997 to 1998, and since 1998 he has been serving as an Adviser of that Technical Group. He received a Best Paper Award of the IEICE in 1999, and IEEE Third Millennium Medal in 2000. He also received a Distinguished Service Award for IEEE Student Activities in 2006. Prof. Nishihara is a Fellow of IEEE, and a member of EURASIP, European Circuits Society, and Japan Society for Educational Technology.